information

MDPI

Article

Which Signal-to-Noise Ratio Is Used in Simulations? Transmitter Side versus Receiver Side: A Study Based on Long Term Evolution Downlink Transmission †

Yu-Sun Liu [1], Shingchern D. You [2,*], Zong-Ru Jhan [3] and Meng-Fan Li [4]

[1] Department of Electronic Engineering, National Taipei University of Technology, Taipei 10608, Taiwan; ysliu@ntut.edu.tw
[2] Department of Computer Science and Information Engineering, National Taipei University of Technology, Taipei 10608, Taiwan
[3] Research and Development Department, Actiontec Electronics, Inc., Taipei 106, Taiwan; jjhan@actiontec.com
[4] Software Development Department, A-MTK Co., Ltd., New Taipei City 235, Taiwan; fan.lee@a-mtk.com.tw
* Correspondence: scyou@ntut.edu.tw
† This paper is an extended version of our paper published at the 11th EAI International Wireless Internet Conference, WiCOM 18, Taipei, Taiwan, 15–16 October 2018.

Abstract: The bit error rate (BER) in relation to the signal-to-noise ratio (SNR) serves as a widely recognized metric for assessing the performance of communication systems. The concept of SNR is so integral that many existing studies presume its definition to be understood, often omitting the specifics of its calculation in their simulations. Notably, the computation of SNR from the perspective of the transmitter yields distinct behaviors and outcomes compared to that from the receiver's side, particularly when the channel encompasses more than mere noise. Typically, research papers utilize the transmitter-side (or ensemble-average) SNR to benchmark the BER performance across various methodologies. Conversely, the receiver-side (or short-term) SNR becomes pertinent when prioritizing the receiver's performance. In the context of simulating the long-term evolution (LTE) downlink, applying both SNR calculation approaches reveals that the receiver-side SNR not only produces a significantly lower BER compared to the transmitter-side SNR but also alters the relative BER performance rankings among the channel models tested. It is deduced that while the transmitter-side SNR is apt for broad performance comparisons, it falls short in thoroughly examining the BER behavior of a receiver across varying SNR scenarios. Therefore, the transmitter-side SNR is useful when comparing the performance of the simulated system with other studies. Conversely, if the primary concern is the actual BER performance of the receiver, the receiver-side SNR could provide a more accurate performance assessment.

Keywords: long-term evolution; signal-to-noise ratio; ergodic channel

check for updates

Citation: Liu, Y.-S.; You, S.D.; Jhan, Z.-R.; Li, M.-F. Which Signal-to-Noise Ratio Is Used in Simulations? Transmitter Side versus Receiver Side: A Study Based on Long Term Evolution Downlink Transmission. *Information* **2024**, *15*, 479. https://doi.org/10.3390/info15080479

Academic Editors: Webert Montlouis, Agbotiname Lucky Imoize and Cheng-Chi Lee

Received: 23 July 2024
Revised: 9 August 2024
Accepted: 10 August 2024
Published: 13 August 2024

Copyright: © 2024 by the authors. Licensee MDPI, Basel, Switzerland. This article is an open access article distributed under the terms and conditions of the Creative Commons Attribution (CC BY) license (https://creativecommons.org/licenses/by/4.0/).

1. Introduction

Nowadays, nearly all communication engineers depend on computer simulations to assess the performance of digital communication systems. One of the fundamental parameters used in these simulations is the signal-to-noise ratio (SNR) [1]. SNR, which is the ratio of signal power to noise power, is so commonly understood that many technical papers do not fully explain how this value is derived during simulations.

Consider the following simple example in Figure 1. It consists of a transmitter, a channel model, a noise source, and a receiver. To calculate the SNR used in the experiments, it is typically assumed that the mean effective gain of antennas [2] is known. For instance, unity for a single-input single-output (SISO) system. During simulations of a SISO system, even though the gain of the antenna is unity, the simulated channel also incurs a gain, known as channel (power) gain [3]. Please refer to Section 2 for details. In the following,

we will use a unity (average) channel gain in the discussion. Under this assumption, the SNR is computed as the ratio of transmitted signal power to noise power (please refer to Section 2 for more details).

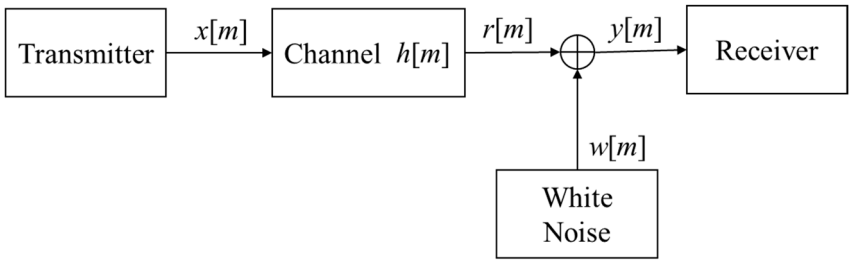

Figure 1. A simple simulated communication system.

However, in a standard simulation procedure, the simulated channel is generated multiple times, such as 50 times (trials) [4]. Each time, the generated channel exhibits different behavior, resulting in varying channel gains from one trial to another (see Section 2 for details). Although the channel gain is no longer unity for each trial, the average channel gain remains close to one, provided a sufficient number of trials are conducted. From the perspective of communication theory, performing averaging over various realizations in a random process is an ensemble average. In this case, the calculation of SNR remains the ratio of transmitted signal power to noise power. This is the standard method for computing SNR in almost all research papers.

As mentioned previously, the channel gain varies across different trials. In some trials, the channel gain can significantly deviate from unity, such as 0.8 or 1.2. In this situation, there are two possible ways to compute the SNR. The first method is the conventional one, which uses the transmitted signal power as the denominator in the SNR calculation. This method computes the SNR from the viewpoint of the transmitter side, essentially using the ensemble average of received signal power as a basis. The second method uses the average power of the received signal for that specific trial as the denominator, computing the SNR from the receiver's perspective over a short period.

Theoretically, if the channel is ergodic [5], then after averaging over a very long period, both SNR values should be equal. Unfortunately, as we will demonstrate through simulations, many orthogonal frequency-division multiplexing (OFDM)-based communication systems [6] do not have sufficiently long codewords for the time average to approach the ensemble average. In the following discussion, we will refer to the transmitter-side SNR as the ensemble-average SNR and the receiver-side SNR as the short-term SNR. Please refer to Section 2 for a complete description.

It seems reasonable to assume that using either ensemble-average SNR or short-term SNR would not significantly alter the observed performance. Consequently, most existing literature does not explicitly explain how the SNR is calculated. We initially shared this belief. However, during our simulations on the bit error rate (BER) performance of long-term evolution (LTE) downlink (DL) transmission [7–11] over three widely used channel models—the Extended Pedestrian A model (EPA), Extended Vehicular A model (EVA), and Extended Typical Urban model (ETU) [12], defined by the European Telecommunications Standards Institute (ETSI) to represent short, medium, and long delay spread environments, respectively—we discovered some intriguing results. Our simulations revealed that the performance ranking of the three channels would be reversed when switching from ensemble-average SNR to short-term SNR. After an in-depth study, we found that the method used to calculate the SNR value significantly affects the BER performance in the mentioned ETSI channel models. Previously, a portion of the results was published in [4]. In this paper, we aim to share our newest findings on this issue and provide recommendations on the use of SNR in simulations.

The rest of the paper is organized as follows: Section 2 introduces the channel models and the two different definitions of SNR, namely ensemble-average SNR and short-term

SNR. Section 3 describes the LTE DL physical layer. Section 4 outlines the simulation method that uses ensemble-average SNR as the basis for comparison and analyzes the distributions of channel frequency responses. Section 5 details the simulation method that uses short-term SNR as the basis for comparison and discusses the differences in BER performances based on the two SNR calculation methods. Finally, Section 6 summarizes the conclusions.

2. SNR Definition and Channel Models

Referring to Figure 1, the transmitter-side SNR for a particular channel realization is defined as

$$\text{SNR} = 10\log \frac{P_{\text{signal}}}{P_N} \tag{1}$$

where P_{signal} is the power of $x[n]$ and P_N is the power of $w[n]$. On the other hand, the receiver-side SNR is defined as

$$\text{SNR} = 10\log \frac{P_r}{P_N} \tag{2}$$

where P_r is the signal power of $r[n]$. Further details on the calculation of P_{signal}, P_r, and P_N will be provided later in this section.

As previously stated, (1) equals (2) if the channel power gain in Figure 1 is one. To gain more insights into the channel gain, we need to describe the characteristics of a simulation channel. The multipath fading phenomenon in a mobile wireless channel is typically modeled as a tapped delay line [13,14] with a constant delay for each tap. Specifically, the channel impulse response is modeled as:

$$h(t) = \sum_{l=0}^{L-1} h_l \delta(t - \tau_l) \tag{3}$$

where L is the number of paths in the channel, and h_l and τ_l are the complex gain and the delay of path l, respectively. Each τ_l is a constant, and each h_l is an outcome of a complex-valued random variable $\boldsymbol{h_l}$. Since uncorrelated scattering among paths is usually assumed in channel simulation, all $\boldsymbol{h_l}$ are independent random variables. This model is also implemented as the wireless channel in simulations.

As mentioned previously, ETSI defined three channel models—EPA, EVA, and ETU—for LTE DL simulations. The power-delay profiles of these models are listed in Table 1 [12]. It is observed that the EPA model has a much shorter delay spread than the EVA and ETU models. Additionally, the sum of average powers over all taps is not 0 dB. During simulations, however, a normalization procedure is carried out to ensure that the expected value of the channel power gain is one. Specifically, let P_l denote the power of the lth tap listed in the table. The normalized power for each tap is given by

$$\widetilde{p}_l = \frac{P_l}{\sum_{l=0}^{L-1} P_l} \tag{4}$$

To generate a channel, the complex gains h_l, $l = 0, 1, \ldots, L-1$, are obtained as outcomes from independent complex Gaussian random variables $\boldsymbol{h_l}$. Each of these complex random variables has independent and identically distributed (i.i.d.) Gaussian random variables in real and imaginary parts, with a mean of zero and a variance of $\widetilde{p}_l/2$. For example, $\widetilde{p}_0 \approx 1/(1 + 0.794 + 0.631 + 0.501 + 0.158 + 0.019 + 0.08) = 0.314$ for tap 1 in the EPA channel. Note that the values in the denominator are converted from dB (power). When applying (3) to the EPA model, $\tau_0 = 0$, $\tau_1 = 30$ ns, etc., and $E[\boldsymbol{h_0}\boldsymbol{h_0^*}] = \widetilde{p}_0 = 0.314$ for tap 1, $E[\boldsymbol{h_1}\boldsymbol{h_1^*}] = \widetilde{p}_1 = 0.249$ for tap 2, etc., where $E[\cdot]$ denotes the expectation operation and * denotes a complex conjugation.

To conduct a simulated experiment, the trial is repeatedly carried out to produce different sets of h_l. In the following, we refer to a set of h_l produced in one probability trial

as one realization of the channel impulse response. In the simulations, unless otherwise specified, we set the speed to 0.01 km/h so that the channel impulse response remains almost unchanged within the duration of the transmitted signal.

Table 1. Channel profiles.

	EPA Model		**EVA Model**		**ETU Model**	
Tap l	τ_l **(ns)**	P_l **(dB)**	τ_l **(ns)**	P_l **(dB)**	τ_l **(ns)**	P_l **(dB)**
1	0	0.0	0	0.0	0	−1.0
2	30	−1.0	30	−1.5	50	−1.0
3	70	−2.0	150	−1.4	120	−1.0
4	90	−3.0	310	−3.6	200	0.0
5	110	−8.0	370	−0.6	230	0.0
6	190	−17.2	710	−9.1	500	0.0
7	410	−20.8	1090	−7.1	1600	−3.0
8	N/A	N/A	1730	−12.0	2300	−5.0
9	N/A	N/A	2510	−16.9	5000	−7.0

Referring to Figure 1, if the cyclic prefix (CP) is longer than the maximum delay of the multipath channel, the received signal within an OFDM symbol can be expressed as:

$$y[m] = x[m] \bigotimes h[m] + w[m] \tag{5}$$

where $\otimes$ denotes the circular convolution, $x[m]$ and $h[m]$ are the sampled versions of the transmitted OFDM signal and channel impulse response, respectively, and $w[m]$ is the complex-valued additive white Gaussian noise (AWGN) with mean zero and variance $N_0/2$. By applying discrete Fourier transformation (DFT) to $y[m]$, the frequency-domain representation of the received signal at OFDM symbol n and subcarrier k is given by

$$Y[n,k] = X[n,k]H[n,k] + W[n,k] \tag{6}$$

where $Y[n,k]$, $X[n,k]$, $H[n,k]$, and $W[n,k]$ are transformed results of $y[m]$, $x[m]$, $h[m]$, and $w[m]$, respectively. In this paper, we assume that perfect side information, such as channel impulse response, signal power, and noise power, is available to the receiver.

The transmitted signal power in Figure 1 is calculated as

$$P_{\text{signal}} = \lim_{M\to\infty} \frac{1}{2M+1} \sum_{m=-M}^{M} |x[m]|^2. \tag{7}$$

For finite-length signals, the limiting process is omitted. The transmitter-side SNR can then be computed as the ratio of the transmitted signal power P_{signal} to the noise power, as shown in (1), assuming the channel gain is unity. However, since the mentioned channel models are probabilistic, the channel power gain

$$\sum_{l=0}^{L-1} h_l {h_l}^* \tag{8}$$

varies from one channel realization to another. Only by averaging over an infinite number of channel realizations can the channel gain be normalized to unity, as per the procedure in (4). In typical simulation scenarios, with a large number of trials (e.g., 50 trials), the averaged channel power gain approaches one. Thus, the SNR is usually calculated under the assumption of a unity channel gain [11,15,16]. It has been demonstrated that the resulting experimental BER performance aligns with the analytical predictions well [15,16]. Since this SNR is calculated based on the ensemble average of the channel gain, it is appropriately referred to as the ensemble-average SNR.

It is also possible to use the individual channel gain of each realization to compute the receiver-side SNR. First, we compute the signal power $r[m]$ at the receiver side (referring to Figure 1) as:

$$P_{\mathrm{r}} = \frac{1}{|\boldsymbol{M}|} \sum_{m \in \boldsymbol{M}} |x[m] \bigotimes h[m]|^2 \tag{9}$$

where $\boldsymbol{M}$ is the set of sample indexes in a codeword, and $|\boldsymbol{M}|$ is its cardinality. The SNR is then computed as the ratio of P_{r} to the noise power, as shown in (2). Since this SNR is calculated based on a specific channel realization, and typically the codewords are short, we refer to it as short-term SNR.

It is important to note that in an experiment, if we aim to generate channel realizations based on a given short-term SNR value and a fixed noise power (and thus a fixed P_{r}), h_{L-1} will depend on h_0, h_1,..., h_{L-2}, which violates the assumption of uncorrelated scattering in the channel model. Additionally, the theoretical BER analysis developed in [15,16] cannot be directly applied in this case.

In terms of user experience, the short-term SNR is a more accurate indicator as it determines the short-term BER at the user's device. A technique known as effective exponential SNR mapping (EESM) [17,18] has been proposed to convert the instantaneous SNR values on subcarriers to an equivalent SNR in an AWGN environment, from which the packet error rate can be derived. This technique can serve as a link-to-system level interface for simulations [19]. The rationale behind using the EESM method, which employs instantaneous SNR (similar to our short-term SNR), is that it provides a more realistic performance indicator for the receiver.

Conceptually, if the fading process is ergodic, the long-term average of SNR converges to the ensemble-average SNR. However, the codeword length for the LTE physical downlink shared channel (PDSCH) is too short to capture the ergodic nature of the channel models (see Section 3 for a description of LTE DL). Consequently, in simulations, we often observe a significant difference between the ensemble-average SNR and the short-term SNR calculated over a codeword, leading to a substantial disparity in the BER performances based on the two different SNR definitions. Therefore, we examine the differences between these two SNR definitions in greater detail in Sections 4 and 5.

3. LTE DL Physical Layer

The LTE system operates using 10 ms radio frames, with each frame containing 10 subframes of 1 ms duration [20]. Each subframe is divided into two equal-length slots, with each slot comprising seven OFDM symbols, labeled symbol 0 to symbol 6, when a normal CP is used. The time-frequency representation of a DL subframe is depicted in Figure 2, where each small cell represents one subcarrier in one OFDM symbol period. Pilots, indicated by green cells, are inserted in the first and third last OFDM symbols of each slot with a frequency domain spacing of six subcarriers. There is no power boosting in pilot subcarriers. The basic unit for resource allocation is the physical resource block (PRB), which consists of 12 consecutive subcarriers in one slot. This paper considers an LTE system with a 10 MHz bandwidth/50 PRBs, comprising 600 subcarriers (excluding DC).

In DL transmission, data are carried in the PDSCH in units of transport blocks. Each transport block is first segmented into code blocks if its size exceeds 6144 bits. Each code block is then encoded with a rate-1/3 symmetric turbo code, which is the parallel concatenation of two identical 8-state (1, 15/13) constituent codes. Finally, the coded sequence of each code block is processed by a rate-matching module, which adjusts the total number of coded bits in a transport block to match the number of bits supported by the assigned PRBs. In the following simulation experiments, a subframe, comprising 50 PRBs/600 subcarriers in both slots, is assigned to one transport block of length 1408 bits (transmitted using one codeword). Note that the resources available to the PDSCH do not include the pilots and the first three OFDM symbols in each subframe, as shown in Figure 2, since these symbols are occupied by the control channel. Finally, the coded bits are modulated using the QPSK scheme and then transmitted using OFDM with system

parameters listed in Table 2. The resulting code rate is 0.11175, which is close to the lowest rate supported by the LTE standard.

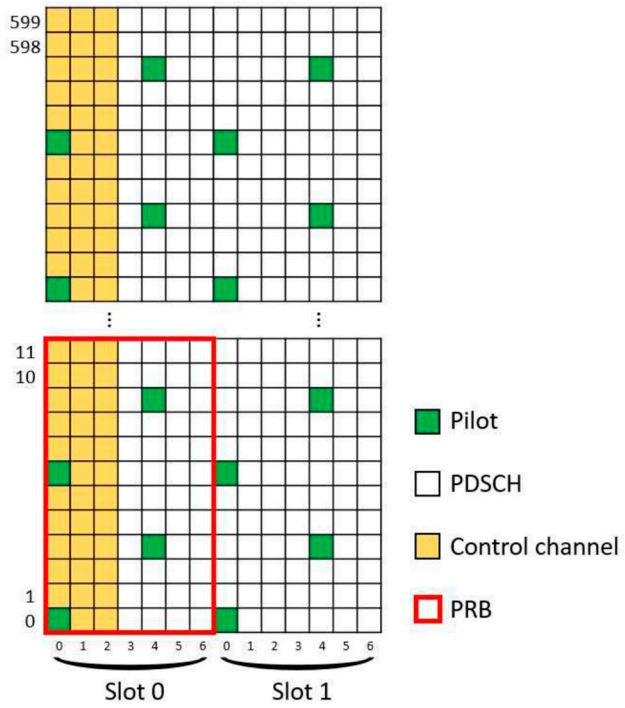

Figure 2. Time-frequency representation of a DL subframe.

Table 2. System parameters.

Parameter	Value
Channel bandwidth	10 MHz
Carrier frequency	1.8 GHz
Subcarrier spacing	15 KHz
Sampling frequency	30.72 M
FFT size	2048
CP duration (NORMAL CP)	160 samples for symbol 0 144 samples for symbols 1–6
OFDM symbol duration	66.6 µs
TX/RX antenna	SISO
Modulation scheme for PDSCH	QPSK
Code rate	0.11175

To conduct the experiments, we use MATLAB to implement both the transmitter and the receiver. A simple receiver diagram is shown in Figure 3. The incoming OFDM signal contains a cyclic prefix (CP), which needs to be removed. Then, a fast Fourier transform (FFT) is performed to obtain the subcarriers. To mitigate the impact of the wireless channel, we use perfect channel estimation and compensation in the experiments. This is followed by a resource element demapper, which constructs resource blocks. Next, a soft demapper is used. In the experiments, QPSK modulation is employed, making the demapping process straightforward. The subsequent step is derate matching, which includes debit selection and pruning, bit separation, and subblock deinterleaving. The final component is a turbo decoder, used for error correction decoding.

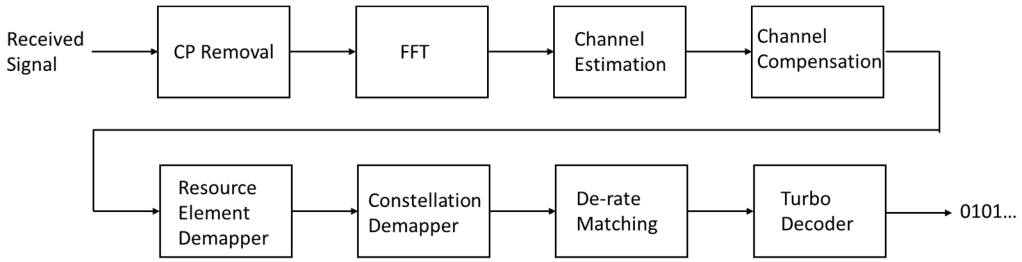

Figure 3. A block diagram of the receiver used in simulations.

4. Experiments with Ensemble-Average SNR

We now describe the procedure for performing simulations with a given ensemble-average SNR value. Essentially, an experiment for a specified SNR value consists of at least 50 trials. In each trial, a new realization of the specified channel model is generated. The noise power is calculated based on the average signal power in (7), the given SNR value, and the assumption of unity channel gain. The reported BER is computed by averaging the BER over all trials.

Following this procedure, we conducted an experiment with 10,000 trials, each corresponding to the duration of one DL frame. In the experiment, each value of $|H[n,k]|$, for all n and k in all trials, is used as a realization of the magnitude of channel frequency response to obtain the empirical probability density function (pdf) of $|\boldsymbol{H}[\cdot,\,\cdot]|$. Figure 4 shows the pdfs of the magnitude of the channel frequency response (i.e., $|H[n,k]|$), derived from the 10,000 trials mentioned earlier, for the three studied channel models. Each pdf plot is obtained from the contour of a histogram with a bin width of 0.01. Recall that perfect side information is assumed to be available; therefore, no channel estimation is performed in the experiments. For a more realistic evaluation, advanced channel estimation methods could be utilized [21,22].

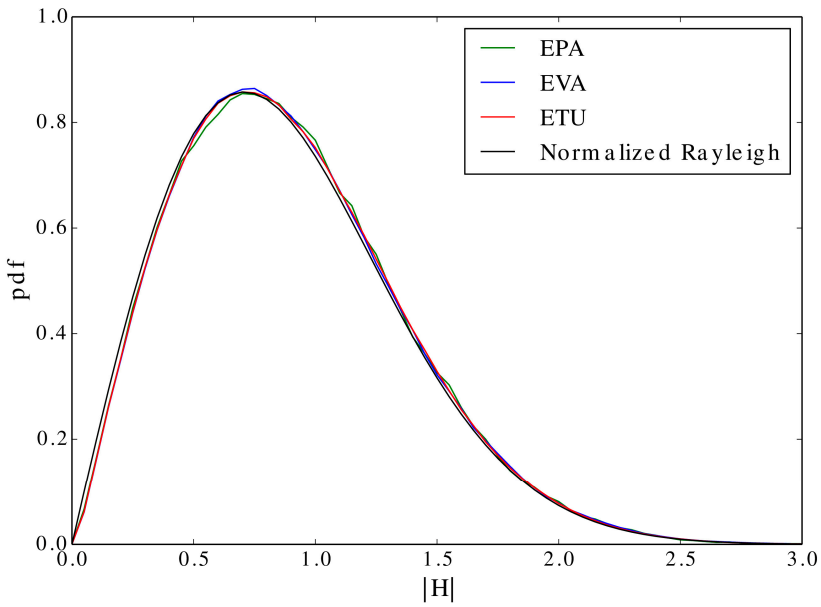

Figure 4. Theoretical and empirical pdfs of the magnitude of channel frequency response.

From Figure 4, we observe that the three empirical pdfs are almost identical. Since $\boldsymbol{H}[n,\,k]$ is the DFT of the sampled version of channel impulse response, $\boldsymbol{H}[n,\,k]$ is a linear combination of path gains, $\boldsymbol{h}_l$, $l = 0, 1, \ldots, L-1$. Thus, it is straightforward to prove that $|\boldsymbol{H}[n,\,k]|$ has a normalized Rayleigh distribution (with unity ensemble-average power gain) for all three channel models, which is confirmed by the figure.

Using the same experiment setup, we also obtained the BER performance after demodulation (referred to as the demodulated BER), and the results are plotted in Figure 5. It is observed that all three channel models yield the same demodulated BER performance. As the three models have the same statistical distribution for the magnitude of channel frequency response, this result is predictable. It is known that the analytical BER of QPSK modulation via a Rayleigh fading channel [23] is

$$\text{BER}_{\text{QPSK, Rayleigh}} = \frac{1}{2}\left(1 - \sqrt{\frac{E_b/N_0}{1 + E_b/N_0}}\right) \tag{10}$$

where E_b is the average energy of each coded bit. For example, if SNR = 0 dB, then $E_b/N_0 = \frac{2048}{600} \cdot \frac{1}{2} = 1.71$, where $\frac{2048}{600}$ is the ratio of FFT size to active subcarriers. Therefore, $\text{BER}_{\text{QPSK, Rayleigh}} = \frac{1}{2}\left(1 - \sqrt{\frac{1.71}{1+1.71}}\right) = 0.10$. To be complete, the analytic results are also plotted in Figure 5. The high degree of agreement between theoretic and experimental results in Figures 4 and 5 confirms the correctness of the simulation program. Since $|\boldsymbol{H}[n, k]|$ has been proven to have a normalized Rayleigh distribution for all three channel models, the simulation BERs agree with the analytical BERs.

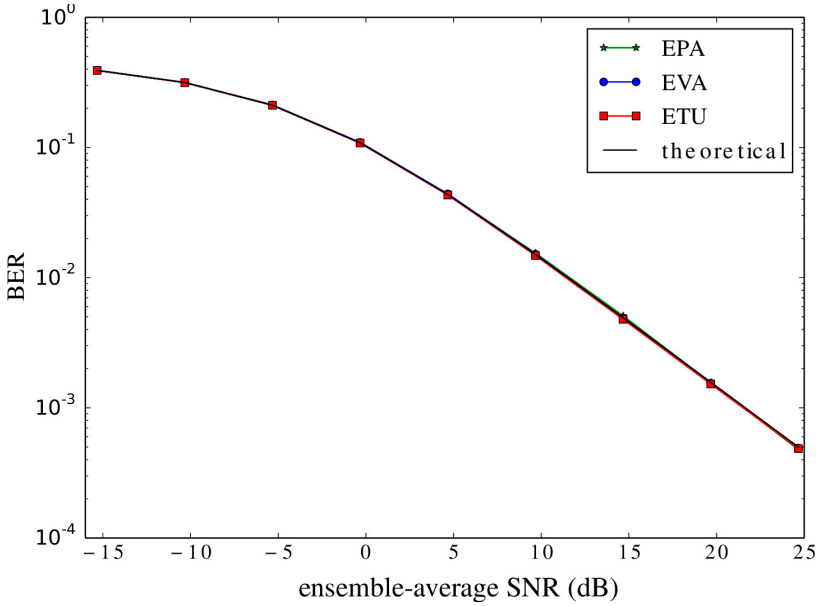

Figure 5. Demodulated BERs using the ensemble-average SNR as a basis of comparison.

Figures 4 and 5 illustrate that all three simulated channels exhibit the same probabilistic characteristics and demodulated BER, regardless of the channels' delay profiles. Different results will be observed when applying the short-term SNR to repeat the same experiment in Section 5.

Using the MATLAB code that implements the receiver shown in Figure 3, we obtain the BER performance after decoding (referred to as the decoded BER throughout this paper), as presented in Figure 6. It is observed that the BERs for all three channels are different. This outcome is counter-intuitive. Given that the three channel models produce identical demodulated BER performance, one would expect similar decoded BER performances as well (after six decoding iterations). However, Figure 6 shows significant variation among the channels. Notably, the decoded BER for the EPA channel model is substantially higher than those for the EVA and ETU models. Furthermore, if a particular channel model were to result in a significantly higher decoded BER, one would expect it to be the ETU model, due to its longer delay spread compared to the CP, which leads to inter-symbol interference (ISI). It is worth mentioning that our previous research on Worldwide Interoperability for Microwave Access (WiMAX) [15] also demonstrated that different channel models yield similar decoded BER performances, within the bounds of experimental uncertainty.

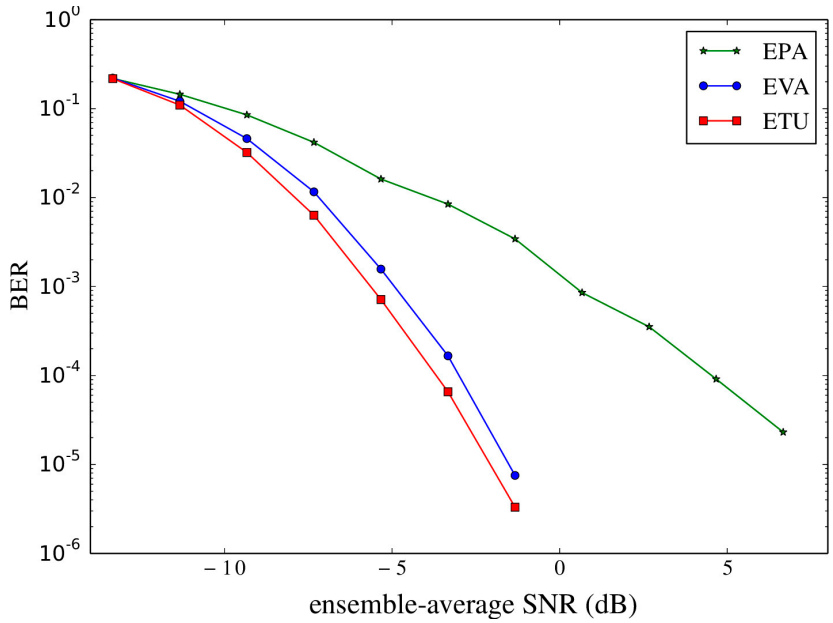

Figure 6. Decoded BERs using ensemble-average SNR as a basis of comparison.

Upon conducting in-depth studies, we discovered that the disparity between the demodulated and decoded BERs is caused by the collective distribution of $|H[n,k]|$ across channel realizations. To simplify the discussion, let $H^{(i)}[n,k]$ denote the realization of the channel frequency response random process $\boldsymbol{H}[n,\ k]$ at the ith trial. By averaging the power gains of all 2048 subcarriers in an OFDM symbol, we obtain

$$\overline{|\boldsymbol{H}[n,\cdot]|^2} = \frac{1}{2048}\sum_{k=0}^{2047}|\boldsymbol{H}[n,k]|^2. \tag{11}$$

According to Parseval's theorem [24]:

$$\overline{|\boldsymbol{H}[n,\cdot]|^2} = \sum_{l=0}^{L-1}|\boldsymbol{h}_l|^2 \tag{12}$$

Since the magnitude of path gain $|\boldsymbol{h}_l|$ is a Rayleigh random variable with parameter $\sigma^2 = \widetilde{p}_l/2$, the random variable $\boldsymbol{Z}_l = |\boldsymbol{h}_l|^2$ is an exponential random variable with mean $\widetilde{p}_l$. Thus, the moment generation function of $\overline{|\boldsymbol{H}[n,\cdot]|^2}$ is given by

$$M(t) = \prod_{l=0}^{L-1}\frac{1}{1-\widetilde{p}_l t} \tag{13}$$

From this, it follows that the mean and variance of $\overline{|\boldsymbol{H}[n,\cdot]|^2}$ are

$$\mathrm{E}[\overline{|\boldsymbol{H}[n,\cdot]|^2}] = \sum_{l=0}^{L-1}\widetilde{p}_l = 1 \tag{14}$$

and

$$\mathrm{Var}[\overline{|\boldsymbol{H}[n,\cdot]|^2}] = \sum_{l=0}^{L-1}\widetilde{p}_l^{\,2} \tag{15}$$

respectively. Recall that, following (4), we have $\widetilde{p}_0 = 0.314$ and $\widetilde{p}_1 = 0.249$ for the EPA channel. Using (15), we have $\mathrm{Var}[\overline{|\boldsymbol{H}[n,\cdot]|^2}] = 0.237$. With further calculations, we obtain variances approximately equal to 0.177 and 0.129 for the EVA and ETU channel models,

respectively. According to (4) and (15), a channel with more evenly distributed power on each tap has smaller $\mathrm{Var}[\overline{|\boldsymbol{H}[n,\cdot]|^2}]$.

To validate our analysis, we plot the theoretical and empirical pdfs of $\overline{|\boldsymbol{H}[n,\cdot]|^2}$ in Figure 7 for the three channel models. The theoretical pdf of $\overline{|\boldsymbol{H}[n,\cdot]|^2}$ is computed by convolving pdfs of L exponential random variables $\boldsymbol{Z}_l$, $l = 0, 1, \ldots, L-1$. The empirical pdf of $\overline{|\boldsymbol{H}[n,\cdot]|^2}$ is obtained using

$$\overline{\left|H^{(i)}[n,\cdot]\right|^2} = \frac{1}{K}\sum_{k=0}^{K-1} |H^{(i)}[n,k]|^2 \tag{16}$$

in each trial i as a realization. In the figure, both $K = 2048$ and $K = 600$ are considered for empirical pdf plots. In the $K = 2048$ case, $\overline{\left|H^{(i)}[n,\cdot]\right|^2}$ in (16) is an average over all subcarriers; in the $K = 600$ case, it is an average over the 600 subcarriers assigned to a transport block. Note that the theoretical and empirical pdfs for 2048 subcarriers are very close to each other, as predicted by (11) and (12).

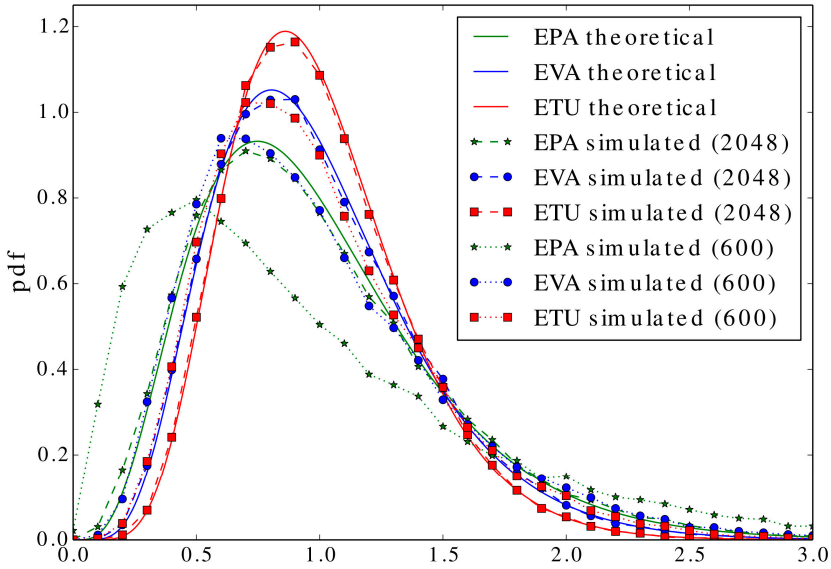

Figure 7. Theoretical and empirical pdfs of $\overline{|\boldsymbol{H}[n,\cdot]|^2}$.

Figure 7 reveals that the EPA model exhibits the widest pdf shape around the mean, while the ETU model has the narrowest shape, as corroborated by their variances. Although we previously demonstrated that the pdfs of the magnitude of the channel frequency response (and thus, the pdfs of subcarrier power gain) for all three channel models are nearly identical (cf. Figure 4), Equation (12) indicates that in a given realization, such as $H^{(i)}[n,k]$, the channel frequency responses of different subcarriers are correlated. Consequently, if $|H^{(i)}[n,k_0]|^2$ is small, it is highly probable that $|H^{(i)}[n,k_1]|^2$ will also be small. As a result, this realization is likely to have a smaller channel gain compared to other realizations.

The difference between the pdfs of $\overline{|\boldsymbol{H}[n,\cdot]|^2}$ for the three channel models becomes more pronounced when $K = 600$. Realizations with small channel gains exhibit low effective SNRs and, consequently, suffer from high decoded BERs. These realizations, therefore, dominate the overall decoded BER performance in the experiment. This phenomenon is more significant in the EPA model compared to the EVA and ETU models, as the EPA model has a larger variance in $\overline{|\boldsymbol{H}[n,\cdot]|^2}$. This larger variance results in more channel realizations with very small channel gains (much less than one), as illustrated in Figure 7. This explains the rationale behind the plots in Figure 6.

In short, a channel with a larger variance, such as EPA in Figure 7, is more likely to have a realization with a channel gain significantly less than one, or a much smaller P_r in (2). Consequently, this channel realization would result in an extremely high decoded BER, as illustrated in Figure 6.

To further illustrate this point, Figure 8 shows examples of $|H[n,k]|$ against subcarriers for the three channel models. It is evident from the figure that (sub)frame 1 is indeed transmitted at much lower power than the other two in the EPA channel. Moreover, in LTE DL transmission, each codeword must fit into a subframe, which is too short to reflect the channel's ergodic nature (if existing), as evidenced by the nonzero variance of $\overline{|\boldsymbol{H}[n,\cdot]|^2}$. Therefore, regardless of how large the ensemble-average SNR is, there is always a nonnegligible probability that the system cannot achieve an arbitrarily small decoded BER. Nevertheless, as the ETU channel has a larger fluctuation of $|\boldsymbol{H}[n,k]|$ over k due to long delay spread, its average power has a higher probability of being close to one.

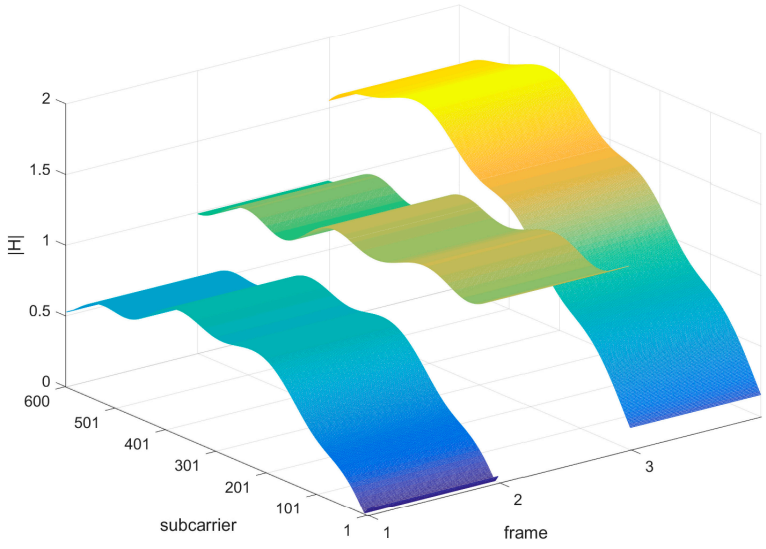

(**a**) EPA

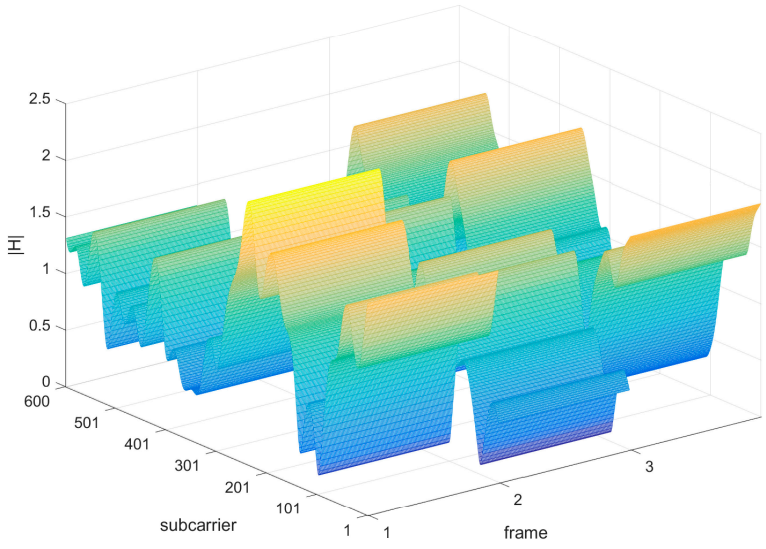

(**b**) EVA

Figure 8. *Cont.*

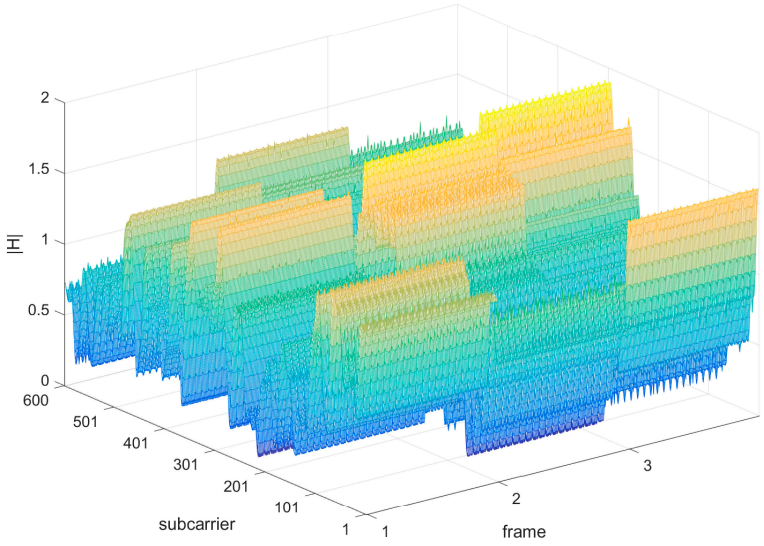

(**c**) ETU

Figure 8. Examples of $|H[n,k]|$ for three trials, each having the duration of one frame.

This phenomenon has been previously observed from the perspective of capacity in [25–27]. It was found that to achieve the Shannon (ergodic) capacity, the length of the codebook must be sufficiently long for the fading channel to exhibit its ergodic nature. If a short codebook is used instead, there is a nonnegligible probability that the actual transmission rate, regardless of how small, will exceed the instantaneous mutual information. This nonnegligible error probability corresponds to the event where some codewords are transmitted at an SNR significantly lower than the ensemble-average SNR.

5. Experiments with Short-Term SNR

In Section 2, we delineated two distinct measurements of SNR: ensemble-average SNR and short-term SNR. The ensemble-average SNR is predominantly utilized in simulations, as it reflects the average performance across numerous channel realizations. However, in practical scenarios, the instantaneous SNR over subcarriers significantly influences the BER at the receiver. Consequently, this instantaneous SNR information, once converted, can be transmitted to the base station to facilitate the adaptation of the modulation and coding scheme (MCS) [17,18]. It is important to note that the short-term SNR discussed in this paper is intrinsically linked to the instantaneous SNR over subcarriers.

We now elucidate the procedure for conducting simulations with a specified short-term SNR value. Again, an experiment for a given SNR value encompasses a substantial number of trials. In each trial, a new realization of the designated channel model is generated, followed by the calculation of noise power based on the received signal power as described in (9) and the given SNR value. The BER is then computed by averaging the BER across all trials.

Using the aforementioned settings and experiments, we obtained the demodulated BER in relation to short-term SNR, as shown in Figure 9. It is observed that the EPA model yields a lower demodulated BER compared to the other two channel models. This is attributed to the EPA model's shorter delay spread, resulting in a smoother channel frequency response. In the EPA model, the value $|H^{(i)}[n,k_0]|^2$ in trial i consistently approximates the average value $\overline{|H^{(i)}[n,\cdot]|^2}$ of the same trial. Conversely, the EVA and ETU channel models occasionally produce significantly lower $\left|H^{(i)}[n,k_0]\right|^2$ values compared to $\overline{|H^{(i)}[n,\cdot]|^2}$,

leading to an increased BER upon demodulation. To justify this claim, Figure 10 illustrates the pdfs of the magnitude of the normalized channel frequency response

$$\boldsymbol{H}'[n,k] = \frac{\boldsymbol{H}[n,k]}{\sqrt{|\boldsymbol{H}[n,\cdot]|^2}} \tag{17}$$

for the three channel models, corroborating our hypothesis. It is observed from Figure 10 that, when compared with the Rayleigh distribution, the pdf corresponding to the EPA channel has a smaller variation (or standard deviation). Therefore, there is a lower probability of encountering significantly lower $|H^{(i)}[n,k_0]|^2$ values.

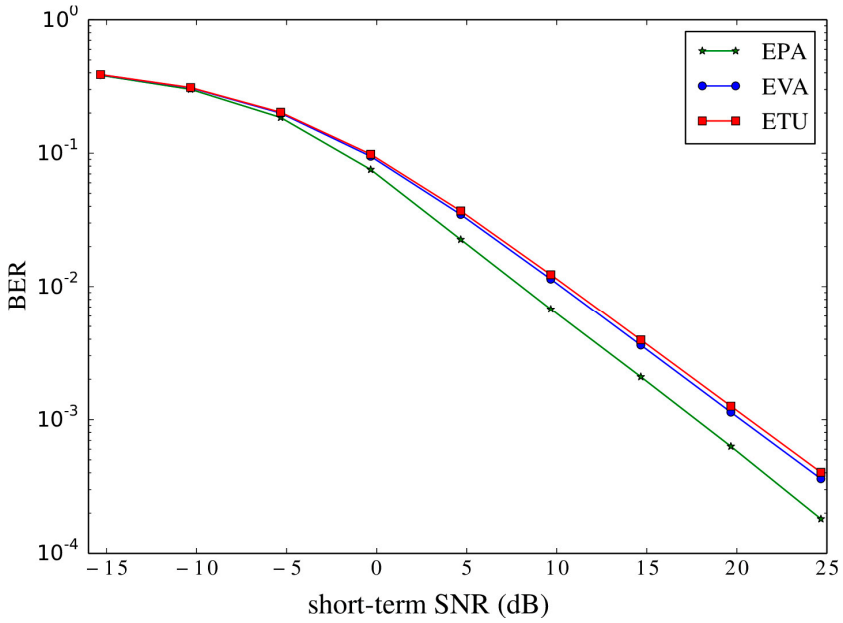

Figure 9. Demodulated BERs using short-term SNR as a basis of comparison.

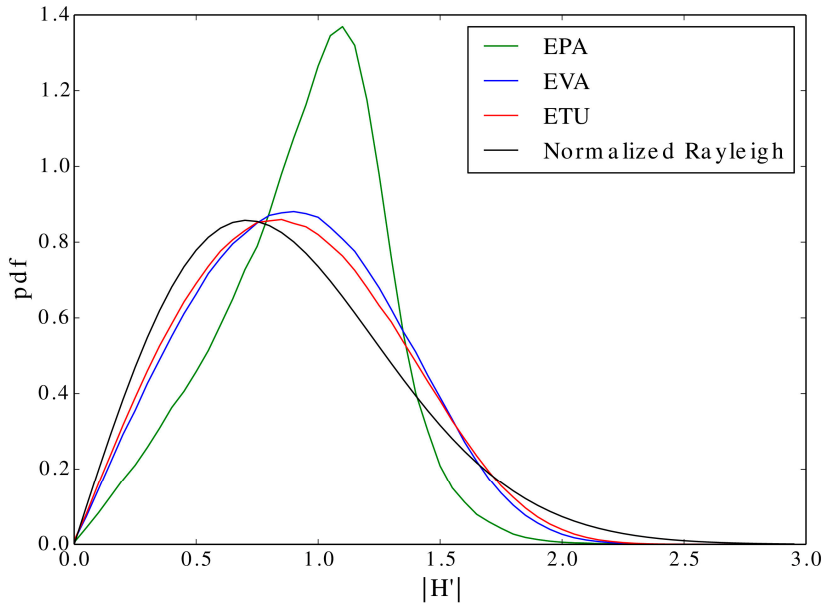

Figure 10. The pdfs of the magnitude of normalized channel frequency response.

In terms of decoded BER (after six decoding iterations), a comparison between Figures 6 and 11 reveals that the BER results derived from short-term SNR are signifi-

cantly lower than those based on ensemble-average SNR. This discrepancy arises because, in the short-term SNR scenario, no single codeword is transmitted through a channel realization with substantially lower instantaneous (effective) SNR. Furthermore, given that source data are transmitted at a very low code rate, the empirical distribution of $|H^{(i)}[n,k]|^2$ has only a minimal impact on the decoded BER, provided that $\overline{\left|H^{(i)}[n,\cdot]\right|^2}$ remains constant. Consequently, the decoded BER performances of the three channel models depicted in Figure 11 are relatively similar. However, among these models, the BER performance of the EPA model most closely approximates that of an AWGN channel due to its lower variance, as illustrated in Figure 10. In contrast, the EPA channel exhibits significantly worse BER performance in Figure 6. This disparity is solely due to the use of different SNR calculations.

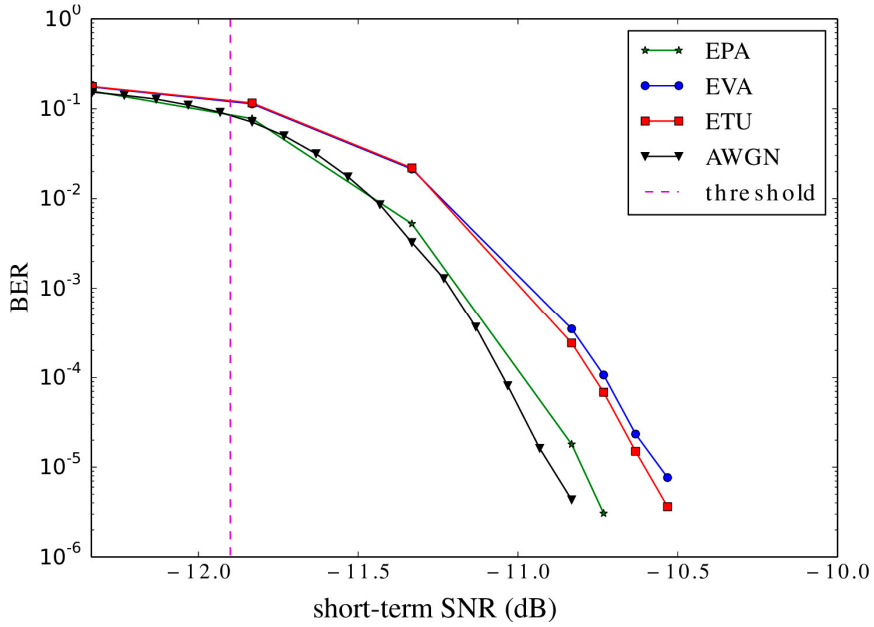

Figure 11. Decoded BERs using short-term SNR as a basis of comparison.

In Figure 11, the convergence threshold of the same turbo code with a code rate of 1/9 for the AWGN channel is also given for comparison. The code rate of 1/9 closely approximates the code rate of 0.11175 used in our experiments. The convergence threshold, as predicted by the extrinsic information transfer (EXIT) chart, represents the minimum SNR required for codewords of infinite length to achieve a very small BER after an infinite number of decoding iterations [28]. Given that the LTE codewords in our experiments have a finite length and the number of decoding iterations is limited to six, it is anticipated that the SNR values corresponding to the waterfall region of the BER curve for the AWGN channel in our experiment will be slightly higher than the convergence threshold, as confirmed by the figure.

To further study the performance of mobile reception, we conducted experiments for both types of SNR at low, medium, and high speeds (3 km/h, 42 km/h, and 180 km/h) with Doppler shifts of 5 Hz, 70 Hz, and 300 Hz, respectively. Figures 12 and 13 illustrate the BER results. It is evident that the ranking of BER performance in the two SNR definitions remains unchanged across low, medium, and high car speeds. Additionally, Figure 12 once again shows counter-intuitive results: the BER performance of the ETU channel at 180 km/h is better than all three channels at lower car speeds. This phenomenon also signifies the need for an alternative SNR definition. On the other hand, the BER performance based on the short-term SNR, shown in Figure 13, behaves as expected: the ETU channel at 180 km/h has the highest BER.

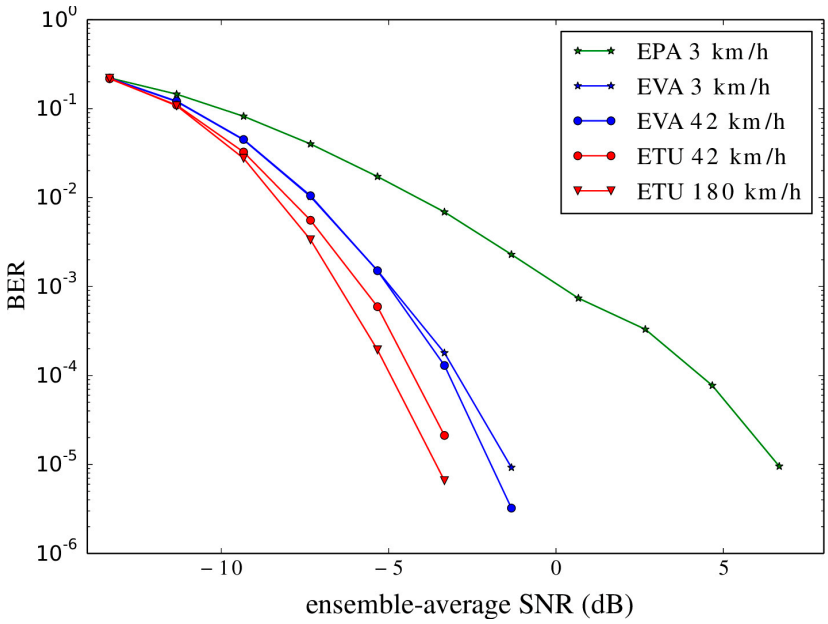

Figure 12. Decoded BERs at low, medium, and high speeds using the ensemble-average SNR as a basis of comparison.

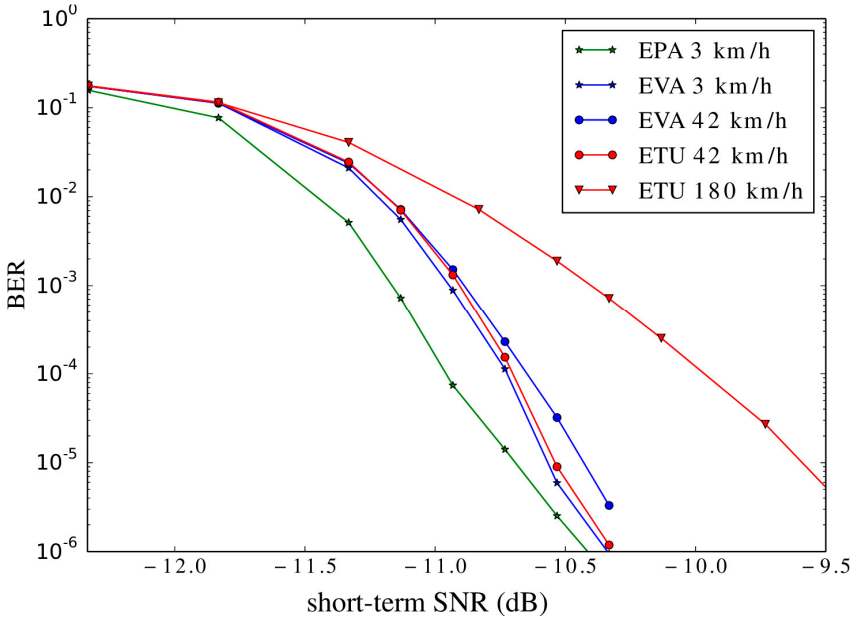

Figure 13. Decoded BERs at low, medium, and high speeds using the short-term SNR as a basis of comparison.

6. Takeaways and Recommendations

In this paper, we examine the impact of different SNR calculation methods on the simulated system performance for the EPA, EVA, and ETU channel models in the LTE DL transmission. It is observed that an LTE subframe is insufficient to capture the long-term ergodic properties (if existing) of these channel models. Specifically, the received signal power averaged over a codeword can significantly differ from the power averaged over an ensemble of channel realizations, a discrepancy that is particularly pronounced in scenarios with small Doppler shifts. Consequently, when the ensemble-average SNR is used in simulations, trials with low channel gain disproportionately influence the overall decoded BER performance. This results in the EPA model, which has a shorter delay spread,

exhibiting higher decoded BER than the EVA and ETU models, which have longer delay spreads, an intuitively counter-intuitive outcome.

In addition to the conventional ensemble-average SNR, we also utilize the short-term SNR to assess the BER performance of the receiver. Simulation results indicate that the short-term SNR not only yields significantly lower decoded BER compared to the ensemble-average SNR for the same channel model but also reverses the relative BER performance rankings among the channel models, aligning with anticipated outcomes. These observations are consistent across low, medium, and high speeds. However, the application of the short-term SNR has its limitations, including the violation of the uncorrelated scattering property in the channel models and difficulties to perform theoretical BER analysis.

Although our experiments were based on LTE downlink simulations, we strongly believe that similar scenarios would arise in other communication systems due to the inherent nature of the SNR calculation. Considering these factors, we recommend using the ensemble-average SNR when comparing the performance of the simulated system with other studies, as this SNR definition is predominantly used in the literature. Conversely, if the primary concern is the actual BER performance of the receiver, the short-term SNR could provide a more accurate performance assessment and should therefore also be evaluated.

Author Contributions: Conceptualization, Y.-S.L. and S.D.Y.; methodology, Y.-S.L.; software, Z.-R.J. and M.-F.L.; formal analysis, Y.-S.L.; writing—original draft preparation, Y.-S.L. and S.D.Y.; writing—review and editing, Y.-S.L. and S.D.Y. All authors have read and agreed to the published version of the manuscript.

Funding: This research was funded by National Science and Technology Council, Taiwan, grant number NSTC 112-2221-E-027-091.

Data Availability Statement: The datasets presented in this article are not readily available because all of the experimental data are generated by a random number generator in the experimental program.

Conflicts of Interest: The authors declare no conflicts of interest.

References

1. Yang, K.; Huang, Z.; Wang, X.; Wang, F. An SNR Estimation Technique Based on Deep Learning. *Electronics* **2019**, *8*, 1139. [CrossRef]
2. Glazunov, A.; Alayon, A.F.M.; Tufvesson, F. Mean effective gain of antennas in a wireless channel. *IET Microw. Antennas Propag.* **2009**, *3*, 214–227. [CrossRef]
3. Lin, Z.; Wang, L.; Ding, J.; Tan, B.; Jin, S. Channel power gain estimation for terahertz vehicle-to-infrastructure networks. *IEEE Commun. Lett.* **2022**, *27*, 155–159. [CrossRef]
4. Liu, Y.-S.; You, S.D.; Jhan, Z.-R.; Li, M.-F. Comparative study of two signal-to-noise ratio calculation methods in LTE downlink simulations. In Proceedings of the Wireless Internet: 11th EAI International Conference, WiCON 2018, Taipei, Taiwan, 15–16 October 2018; pp. 14–23.
5. Adler, R.L. Ergodic and mixing properties of infinite memory channels. *Proc. Am. Math. Soc.* **1961**, *12*, 924–930. [CrossRef]
6. Nee, R.; Prasad, R. *OFDM for Wireless Multimedia Communications*; Artec House: London, UK, 2000.
7. Adegbite, S.; Stewart, B.G.; McMeekin, S.G. Least squares interpolation methods for LTE system channel estimation over extended ITU channels. *Int. J. Inf. Electron. Eng.* **2013**, *3*, 414–418.
8. Weng, F.; Yin, C.; Luo, T. Channel estimation for the downlink of 3GPP-LTE systems. In Proceedings of the 2010 2nd IEEE International Conference on Network Infrastructure and Digital Content, Beijing, China, 24–26 September 2010.
9. Sesia, S.; Toufik, I.; Baker, M. *LTE—The UMTS Long Term Evolution: From Theory to Practice*; John Wiley & Sons: Chichester, UK, 2011.
10. Rumney, M. *LTE and the Evolution to 4G Wireless: Design and Measurement Challenges*, 2nd ed.; John Wiley & Sons: Chichester, UK, 2013.
11. Liu, Y.-S.; You, S.D.; Liu, Y.-M. Iterative channel estimation method for long-term evolution downlink transmission. *IET Commun.* **2015**, *9*, 1906–1914. [CrossRef]
12. 3GPP. *LTE Evolved Universal Terrestrial Radio Access (E-UTRA); User Equipment (UE) Radio Transmission and Reception*; 3GPP TS 36.101; 3GPP: Valbonne, France, 2013.
13. Blazek, T.; Ashury, M.; Mecklenbräuker, C.F.; Smely, D.; Ghiaasi, G. Vehicular channel models: A system level performance analysis of tapped delay line models. In Proceedings of the 2017 15th International Conference on ITS Telecommunications (ITST), Warsaw, Poland, 29–31 May 2017.

14. Hassan, N.; Thomä, R.; Matolak, D.W. In-stationary tapped delay line channel modeling and simulation. In Proceedings of the 2020 14th European Conference on Antennas and Propagation (EuCAP), Copenhagen, Denmark, 15–20 March 2020; pp. 1–5. [CrossRef]
15. You, S.D.; Chen, K.-Y.; Liu, Y.-S. Cubic convolution interpolation function with variable coefficients and its application to channel estimation for IEEE 802.16 initial downlink. *IET Commun.* **2012**, *6*, 1979–1987. [CrossRef]
16. Prasad, R. *OFDM for Wireless Communications Systems*; Artec House: London, UK, 2004.
17. 3GPP. *System-Level Evaluation of OFDM—Further Considerations*; Ericsson, 3GPP TSG-RAN WG1 35, R1-031303; 3GPP: Valbonne, France, 2003.
18. Donthi, S.N.; Mehta, N.B. An accurate model for EESM and its application to analysis of CQI feedback schemes and scheduling in LTE. *IEEE Trans. Wirel. Commun.* **2011**, *10*, 3436–3448. [CrossRef]
19. Paunov, P.; Camargo, A.; Czylwik, A. EESM as a link to system level interface for MIMO OFDM systems based on QOSFBC. In Proceedings of the ITG/IEEE Workshop on Smart Antennas, Vienna, Austria, 26–27 February 2007.
20. Mousavi, H.; Amiri, I.S.; Mostafavi, M.A.; Choon, C.Y. LTE physical layer: Performance analysis and evaluation. *Appl. Comput. Inform.* **2019**, *15*, 34–44. [CrossRef]
21. Liu, Y.-S.; You, S.D.; Lai, Y.-C. Machine Learning-Based Channel Estimation Techniques for ATSC 3.0. *Information* **2024**, *15*, 350. [CrossRef]
22. Oyerinde, O.O.; Flizikowski, A.; Marciniak, T.; Zelenchuk, D.; Ngatched, T.M.N. Compressive Sensing-Based Channel Estimation for Uplink and Downlink Reconfigurable Intelligent Surface-Aided Millimeter Wave Massive MIMO Systems. *Electronics* **2024**, *13*, 2909. [CrossRef]
23. Rao, K.D. *Channel Coding Techniques for Wireless Communications*; Springer: New Delhi, India, 2015.
24. Haykin, S.S.; Van Veen, B. *Signals and Systems*; John Wiley & Sons: Chichester, UK, 1999.
25. Ozarow, L.H.; Shamai, S.; Wyner, A.D. Information theoretic considerations for cellular mobile radio. *IEEE Trans. Veh. Technol.* **1994**, *43*, 359–378. [CrossRef]
26. Biglieri, E.; Proakis, J.; Shamai, S. Fading channels: Information theoretic and communications aspects. *IEEE Trans. Inf. Theory* **1998**, *44*, 2619–2692. [CrossRef]
27. Xiao, C.; Zheng, Y.R. Ergodic capacity, capacity distribution and outage capacity of MIMO time-varying and frequency selective Rayleigh fading channels. In Proceedings of the 41st Annual Allerton Conference on Communication, Control, and Computing, Monticello, UT, USA, 1–3 October 2003.
28. Ten Brink, S. Convergence behavior of iteratively decoded parallel concatenated codes. *IEEE Trans. Commun.* **2001**, *49*, 1727–1737. [CrossRef]

Disclaimer/Publisher's Note: The statements, opinions and data contained in all publications are solely those of the individual author(s) and contributor(s) and not of MDPI and/or the editor(s). MDPI and/or the editor(s) disclaim responsibility for any injury to people or property resulting from any ideas, methods, instructions or products referred to in the content.